Matsubara QSGW+DMFT: application to Mott insulators

Sangkook Choi,[1] Andrey Kutepov,[1] Kristjan Haule,[1] Mark van Schilfgaarde,[2] and Gabriel Kotliar[1]

[1] *Department of Physics and Astronomy, Rutgers University, Piscataway, New Jersey 08854, USA*
[2] *Department of Physics, Kings College London, Strand, London WC2R 2LS, United Kingdom*

(Dated: November 5, 2015)

We present a new *first principles* approach to strongly correlated solids. It is based on a combination of the quasiparticle self-consistent GW approximation and the Dynamical Mean Field Theory (DMFT). The sole input in this method is the projector to the set of localized orbitals for which all local Feynman graphs are being evaluated. For that purpose we choose very localized quasiatomic orbitals spanning large energy window, which contains most strongly-hybridized bands as well as upper and lower Hubbard bands. The self-consistency is carried out on the Matsubara axis. This method enables the first principles study of Mott insulators in both their paramagnetic (PM) and antiferromagnetic (AFM) phase. We illustrate the method on the archetypical charge transfer correlated insulator La_2CuO_4 and NiO, and obtain spectral properties and magnetic moments in good agreement with experiments.

Introduction. The *first principles* description of strongly-correlated materials is currently regarded as one of the greatest challenges in condensed matter physics. The interplay between localized electrons in open d- or f-shell and itinerant band states gives rise to rich physics that makes these materials attractive for a wide range of applications such as oxide electronics, high temperature superconductors and spintronic devices. Various theoretical approaches are currently being pursued [1]. One of the most successful approaches is the dynamical mean field theory (DMFT) [2]. In combination with density functional theory [3, 4], it has described many features of strongly-correlated materials successfully and highlighted the surprising accuracy of treating correlations local to a small subset of orbitals exactly, while treating the reminder of the problem in a static mean field manner.[5, 6].

The numerous successes of DMFT in different classes of correlated materials revived the interest in the long sought goal of achieving a diagrammatically controlled approach to the quantum many body problem of solids, starting from the Green's function G and the screened Coulomb interactions W [7, 8]. The lowest order diagram in perturbation theory in this functional gives rise to the GW approximation [9] while the local approximation applied to the most correlated orbitals gives rise to an extended DMFT approach to the electronic structure problem [8]. The addition of the GW and DMFT graphs was proposed and implemented in model Hamiltonian studies [10] and in realistic electronic structure [11, 12]. There is now intense activity in this area with many recent publications [13–16] triggered by advances in the quality of the impurity solvers [17–19], insights into the analytic form of the high frequency behavior of the self-energy [20] and improved electronic structure codes.

Several conceptual issues remain to be clarified before the long sought goal of a robust electronic structure method for solids is attained. The first issue is the choice of local orbitals on which to perform the DMFT method (summation of all local Feynman graphs). The second issue is the level of self-consistency that should be used in the calculation of various parts of the diagrams included in the treatment (free or bare Green's function G_0 vs self-consistent interacting Green's functions G). These central issues are addressed in this letter.

The self-consistency issue appears already at the lowest order, namely the GW level, and it has been debated over time. The corresponding issue in GW+DMFT is expected to be at least as important, but has not been explored, except for model Hamiltonians [21, 22]. At the GW level, it is now well established that Hedin's fully self-consistent formulation [9], while producing good total energies in solids [23], atoms and molecules [24, 25], does not produce a good approximation to the spectra of even 3D electron gas and aluminum in comparison to non self-consistent GW results [23, 26]. Instead, using a free (quasiparticle) Green's function in the evaluation of the polarization graph of the GW method gives much better results for spectral functions. This is the basis of the one-shot quasiparticle (QP) GW, starting from LDA [27] or from others [28, 29]. Unfortunately, the answer depends on the starting point. A solution for this problem is to impose a self-consistency equation to determine G_0. This method, called the quasiparticle self-consistent GW (QSGW) [30], is very successful reproducing the spectra of many systems [31–33]. How to combine it with DMFT, is an important open challenge [34, 35].

Previous GW+DMFT studies typically used a G_0 which depends on the LDA starting point, and projectors spanning a relatively small energy window [13–16]. In this work, we propose a different approach to the level of self-consistency and the choice of the DMFT orbital. We do a self-consistent QSGW calculation and then calculate local self-energy using DMFT with static U_d and J_H without feedback to non-local self-energy within GW. For the DMFT step, we choose a very localized orbital spanning large energy window which contains most strongly-hybridized bands as well as upper and lower Hubbard

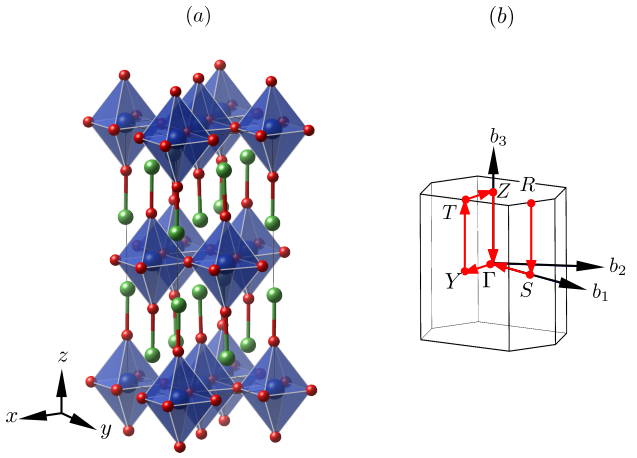

Figure 1. (color online) (a) Atomic structure of La_2CuO_4 in the single face-centered orthorhombic phase. Lanthanum atoms are represented by green spheres, copper atoms by blue spheres in the blue octahedrons, and oxygen atoms by red spheres. The structure is characterized by an alternating rotation of successive CuO_6 octahedra along the x direction. (b) First Brillouin zone of single face-centered orthorhombic phase. Red lines show the path along which electronic bandstructures are plotted in Fig. 2(c) and Fig. 3.

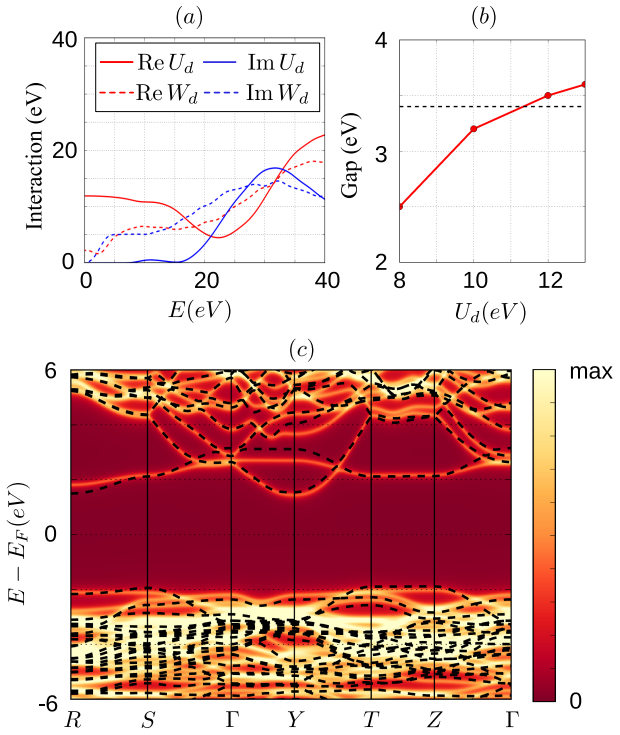

Figure 2. (color online) (a) Frequency dependence of W_d (dashed lines) and U_d (full lines) of La_2CuO_4 with a χ^{low}_{QP} defined in the energy window $E_F \pm 10eV$. Real and imaginary parts of the parameter are marked by red and blue colors, respectively. (b) Bandgap dependence on U_d, in La_2CuO_4, evaluated with impurity self-energy within spin-polarized GW approximation with J_H=1.4eV. The Black dashed line represents bandgap within spin-polarized MQSGW. (c) Spectral function of La_2CuO_4 with U_d=12eV and J_H=1.4eV. The black dashed-lines show bandstructures within spin-polarized MQSGW

bands.

In the LDA+DMFT context, the choice of very localized orbitals has provided a great deal of universality since the interactions do not vary much among compounds of the same family. This has been demonstrated in the studies of iron pnictides [36] and transition metal oxides [37]. This choice results in a second advantage as we will show below, namely the frequency dependence of the interaction matrix can be safely ignored. Having chosen the correlated orbitals, all the other parameters are self-consistently determined. (see Supplemental Material [38] to see how the change of local orbital leads to to changes in the calculated U in a way that they preserve the low energy physics.) This is the first *ab initio* quasiparticle self-consistent GW+DMFT implementation and the first study on a paramagnetic Mott insulator within the GW+DMFT method.

Methods. Our approach is carried it out entirely on the Matsubara axis, which requires a different approach to the quasiparticle self-consistency in GW [39], called Matsubara Quasiparticle Self-consistent GW (MQSGW), where the quasiparticle Hamiltonian is constructed by linearizing the self-energy and renormalization factor [40]. Working on the Matsubara axis, is numerically very stable, provide a natural interface with advanced DMFT solvers such as continuous-time quantum Monte-Carlo (CTQMC) [17–19] and has very good scaling in system size as in the space-time method [41]. (see Supplemental Material [38] for details).

For DMFT, it is essential to obtain bandstructure in a fine enough crystal momentum ($\mathbf{k}$) mesh to attain desired frequency resolution of physical quantities. To achieve such momentum resolution, we use a Wannier-interpolated MQSGW bandstructure in a large energy window using Maximally localized Wannier function (MLWF) [42], and than constructed local projector in a fine momentum mesh. In contrast to $SrVO_3$ [13–16] where a set of t_{2g} states is reasonably well separated from the other bands, correlated $3d$ orbitals in La_2CuO_4 shown in Fig. 1 are strongly hybridized with other itinerant bands. In this case, it is necessary to construct local projectors from states in a wide enough energy windows to make projectors localized near the correlated atoms. We constructed local projectors in the energy window $E_F \pm 10eV$ in which there are ∼82 bands at each $\mathbf{k}$ point, where E_F is the Fermi level. Then we confirmed that absolute value of its overlap to the muffin-tin orbital (of which radial function is determined to maximize electron occupation in it) is more than 95%. Our choice of energy window is justified by the Cu-$3d$ spectra being entirely contained in this win-

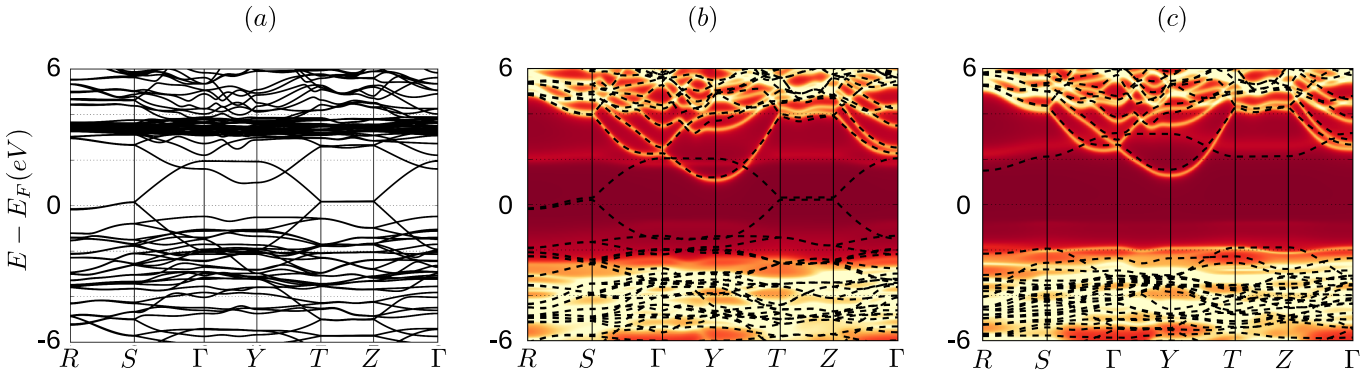

Figure 3. (color online) (a) Electronic bandstructures of La_2CuO_4 within LSDA and spectral functions from (b) non spin-polarized MQSGW+DMFT (c) and spin-polarized MQSGW+DMFT calculations along the path shown in Fig. 1(b). The Dashed lines in (b) and (c) represent electronic bandstructures within non spin-polarized MQSGW and spin-polarized MQSGW, respectively

dow. For $3d$ orbitals in NiO, MLWF are constructed in a energy windows of $E_F - 11eV$ to $E_F + 10eV$. Using constructed MLWFs, we defined our local-projector $P_{i,n}(\mathbf{k}) = \sum_R \langle W_{\mathbf{R}i}|\psi_{n\mathbf{k}}\rangle\, e^{-i\mathbf{k}\cdot\mathbf{R}}/\sqrt{N_k}$, where $W_{\mathbf{R}i}(\mathbf{r})$ is MLWF with an index i, $\psi_{n\mathbf{k}}(\mathbf{r})$ is quasiparticle wavefunction with an index n, and N_k is the number of $\mathbf{k}$ points in the first Brillouin zone.

Static U_d and J_H are evaluated by a modification of the constrained RPA method [43], which avoids screening by the strongly hybridized bands. This screening by hybridization is included in our large energy window DMFT. For details, see Supplemental Material [38]. We divide dynamic polarizability within MQSGW approximation χ_{QP} into two parts, $\chi_{QP} = \chi^{low}_{QP} + \chi^{high}_{QP}$. Here, χ^{low}_{QP} is defined by all transitions between the states in the energy window accounted for by the DMFT method ($E_F \pm 10eV$ for La_2CuO_4 and $E_F - 11eV$ to $E_F + 10eV$ for NiO). Using χ^{high}_{QP}, we evaluate partially screened Coulomb interaction $U^{-1}(\mathbf{r},\mathbf{r}',\mathbf{k},i\omega_n) = V^{-1}(\mathbf{r},\mathbf{r}',\mathbf{k}) - \chi^{high}_{QP}(\mathbf{r},\mathbf{r}',\mathbf{k},i\omega_n)$ and parametrize static U_d and J_H by Slater's integrals [44, 45], where V is bare Coulomb interaction.

The Feynman graphs included in both MQSGW and DMFT (double-counting) are the local Hartree and the local GW diagram. They are computed using the local projection of the MQSGW Green's function ($\hat{G}_{QP}$) $\hat{G}^{loc}_{QP}(i\omega_n) = \frac{1}{N_k}\sum_{\mathbf{k}} \hat{P}(\mathbf{k})\hat{G}_{QP}(\mathbf{k},i\omega_n)\hat{P}^{\dagger}(\mathbf{k})$ and the local Coulomb matrix $U_{iklj} = \int d\mathbf{r}d\mathbf{r}' W^*_{\mathbf{R}=0,i}(\mathbf{r}) W^*_{\mathbf{R}=0,k}(\mathbf{r}')$ $W_{\mathbf{R}=0,l}(\mathbf{r}')W_{\mathbf{R}=0,j}(\mathbf{r})U(\mathbf{r},\mathbf{r}',\mathbf{R}=0,i\omega_n=0)$. For the details, see Supplemental Material [38].

Results. Fig. 2(a) shows the frequency dependence of real and imaginary parts of U_d of La_2CuO_4 (For NiO, see Supplemental Material [38]). It is calculated on an imaginary frequency axis and analytically continued by a maximum entropy method [47]. We also plot the fully screened Coulomb interaction W_d for comparison. Static U_d is 12.0 eV and U_d remains almost constant up to 10 eV. In contrast, in W_d, there are several peaks due to low-energy collective excitations below 10 eV. At very high energy, U_d approaches the bare coulomb interaction of 28 eV. Calculated J_H is 1.4 eV and has negligible frequency dependence. By contrast, conventional constrained-RPA, in which 10 bands of mostly Cu-$3d$ character are excluded from screening, results in static $U_d = 7.6$ eV, which is too small to open the Mott gap, and which is also inconsistent with photoemission experiments on CuO charge transfer insulators [48].

We also computed the static U_d and J_H by requiring that the calculated excitation spectra of La_2CuO_4 within MQSGW+DMFT with (local) GW as the impurity solver matches the spin-polarized MQSGW spectra. Here we used non spin-polarized MQSGW band structure and allowed spontaneous magnetic long range order by embedding impurity self energy, which is function U_d and J_H, within spin-polarized GW approximation. In Fig. 2(b), we allowed U_d to vary between 8-13 eV (at fixed $J_H = 1.4$ eV) and we plot the size of the indirect gap. The gap size of this method matches the gap of spin-polarized MQSGW when $U_d \approx 12$ eV. If the choice of U_d and J_H is correct, the resulting spectra must be similar to the prediction of spin-polarized MQSGW method. We show this comparison in Fig. 2(c) to confirm a good match. In addition, the relative position of Cu-d band (the lowest energy conduction band at S) to the La-d band (the lowest energy conduction band at Y) is also well matched justifying the approximation of $\hat{\Sigma}^{DC}(i\omega_n) \simeq \hat{\Sigma}^{DC}(i\omega_n = 0)$. $\Sigma^{DC}(i\omega_n = 0)$ for Cu-$d_{x^2-y^2}$ orbital differs from nominal double counting energy [49] by only 1%, highligting again the advantages of using a broad window and narrow orbitals.

We now discuss the magnetic moment associated with Cu and the electronic excitation spectra of La_2CuO_4 by using MQSGW+DMFT (with $U_d = 12.0eV$, $J_H = 1.4eV$) in which the impurity is solved by the numerically exact CTQMC [17, 18] and compare them

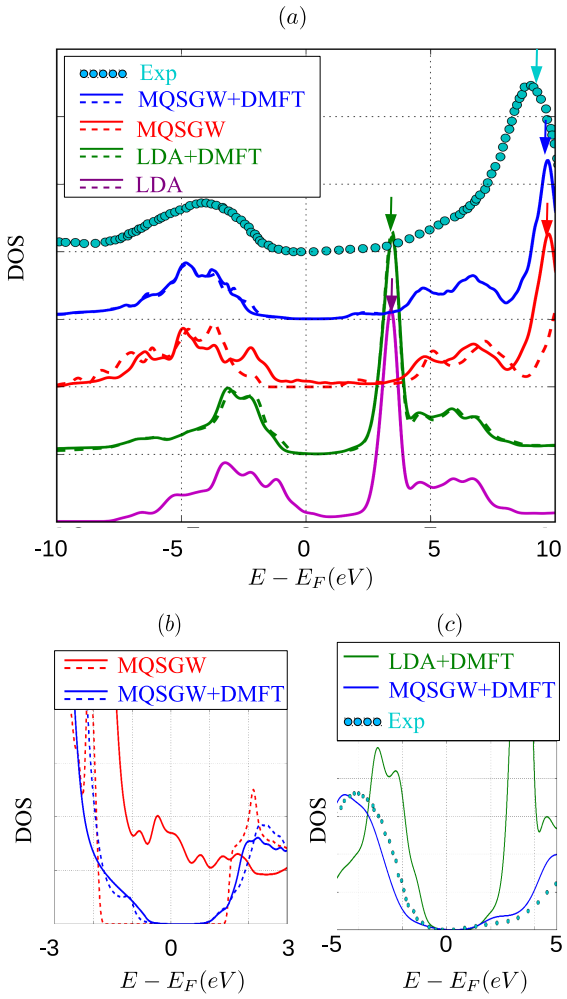

Figure 4. (color online) (a) Total density of states of La_2CuO_4 from LDA (magenta), LDA+DMFT(green), MQSGW (red), and MQSGW+DMFT (blue). Full lines and dashed-lines represent quantities within non spin-polarized and spin-polarized versions of each calculation, respectively. The cyan dotted line shows photoemission/inverse-photoemission data [46]. The Positions of La-f peaks are marked by arrows. (b) A zoom-in view in the low-energy region. (c) The overlap of total density of states of La_2CuO_4 within LDA+DMFT as well as MQSGW+DMFT and photoemission/inverse-photoemission data [46]

with other methods (For NiO, see Supplemental Materials [38]). LSDA does not have a magnetic solution. In contrast, spin-polarized MQSGW, QSGW [30], and MQSGW+DMFT predict 0.7 μ_B, 0.7 μ_B, and 0.8 μ_B, respectively. This is consistent with experimental measurements, although the later span quite large range $0.4\mu_B \sim 0.8\mu_B$ [50–52].

In the low-energy spectrum of La_2CuO_4, LSDA does not have a insulating solution; there is a single non-magnetic solution with zero energy gap as shown in the bandstructure(Fig. 3(a)) and total density of states (Fig. 4(a)). The non spin-polarized MQSGW also predicts metal as shown in Fig. 4(a), but the two bands of primarily $Cu\text{-}d_{x^2-y^2}$ character near the Fermi level are well-separated from the rest of the bands (dashed lines in Fig. 3(b)). Spin-polarized MQSGW calculation (dashed lines in Fig. 3(c)) yields qualitative different results from LSDA and non spin-polarized MQSGW calculation. The two $Cu\text{-}d_{x^2-y^2}$ bands are now well separated from each other with a bandgap of 3.4 eV. Spin-polarized QSGW [30] also yields insulating phase with a gap of 4.0 eV. In the experiment, the larger direct gap, as measured by optics, is $\sim 2eV$ [53, 54].

We show that these deficiencies of LDA, QSGW and MQSGW in the low-energy spectra can be remedied by adding all local Feynman diagrams for the Cu-d orbitals using the DMFT. The LDA+DMFT calculation in Fig. 4(a), carried out by the all-electron LDA+DMFT method [37, 49], predicts reasonable gap of 1.5 eV and 1.8 eV in PM and AFM phases, in good agreement with experiment and previous LDA+DMFT studies [37, 55–58]. Within MQSGW+DMFT, we find gaps of 1.5 eV and 1.6 eV in PM and AFM phases, respectively, as shown in Fig. 4(b). The excitation spectra of MQSGW+DMFT in PM and AFM phase as shown in Fig. 3(b) and 3(c) are very similar as both are insulating with well separated $Cu\text{-}d_{x^2-y^2}$ bands, which is now also substantially broadened due to large scattering rate in Hubbard-like bands. In addition, MQSGW+DMFT improves the line-shape of LDA+DMFT. Near the top of the valence bands with oxygen p character, the lineshape within LDA+DMFT is too sharp in comparison to the experiments as shown in Fig. 4(c). By treating oxygen p levels within GW, the lineshape becomes smoother and in a better agreement with experiments (the lineshape improvement at the top of the valence band are also observed in NiO, see Supplemental Material [38] for details)

In the high energy region of La_2CuO_4, the most distinctive difference is the position of La-f peak. It appears at $\sim 3eV$ within LDA and LDA+DMFT, but at around $\sim 9eV$, in the inverse-photoemission spectra (cyan dotted line in Fig. 4(a)) [46]. By treating La-f within GW approximation, it appears at $\sim 10eV$ within MQSGW and MQSGW+DMFT. The underestimation of unoccupied La-f excitation energy is attributed to the local approximation to the electron self-energy within LDA. Within LDA, Hartree and exchange-correlation potential applied to La-f orbitals are orbital-independent since charge density is averaged over 14 different m channels [59]. In contrast, these potentials within MQSGW are orbital-dependent and non-local. The effect of orbital-dependent potential can be tested within LDA+U approaches, since LDA+U adds orbital-dependent potential and subtracts orbital-independent potential explicitly [3]. From LDA+U approaches, we can also understand MQSGW better since LDA+U can be regarded as a local and static approximation to GW approximation [3]. According to M.T.Czyzyk and G.A.Sawatzky [60],

La-f peaks shift from E_F+3eV to E_F+3eV+U/2 with U=11eV for La-f.

In summary, we introduced a new methodology within MQSGW+DMFT and tested it in the classic charge transfer insulator La_2CuO_4 and NiO. Our methodology predicts a Mott-insulating gap in the PM phase, thus overcoming the limitation of LDA and QSGW. It yields more precise peak positions of the La-f states and valence band lineshape, thus improving the results of LDA+DMFT. The method should be useful in understanding electronic excitation spectrum of other strongly-correlated materials, in particular those where precise position of both the itinerant and correlated states is important.

This work was supported by Simons foundation under project "Many Electron Problem" and computational resources are provided by the Oak Ridge Leadership Computing Facility at the Oak Ridge National Laboratory, which is supported by the Office of Science of the U.S. Department of Energy under Contract No. DE-AC05-00OR22725.

[1] V. I. Anisimov, *Strong Coulomb Correlations in Electronic Structure Calculations* (CRC Press, 2000).
[2] A. Georges, G. Kotliar, W. Krauth, and M. J. Rozenberg, Rev. Mod. Phys. **68**, 13 (1996).
[3] V. I. Anisimov, A. I. Poteryaev, M. A. Korotin, A. O. Anokhin, and G. Kotliar, J. Phys.: Condens. Matter **9**, 7359 (1997).
[4] A. I. Lichtenstein and M. I. Katsnelson, Phys. Rev. B **57**, 6884 (1998).
[5] G. Kotliar, S. Y. Savrasov, K. Haule, V. S. Oudovenko, O. Parcollet, and C. A. Marianetti, Rev. Mod. Phys. **78**, 865 (2006).
[6] K. Held, Advances in Physics **56**, 829 (2007).
[7] C.-O. Almbladh, U. V. Barth, and R. V. Leeuwen, Int. J. Mod. Phys. B **13**, 535 (1999).
[8] R. Chitra and G. Kotliar, Phys. Rev. B **63**, 115110 (2001).
[9] L. Hedin, Phys. Rev. **139**, A796 (1965).
[10] P. Sun and G. Kotliar, Phys. Rev. B **66**, 085120 (2002).
[11] S. Biermann, F. Aryasetiawan, and A. Georges, Phys. Rev. Lett. **90**, 086402 (2003).
[12] G. Kotliar and S. Y. Savrasov, in *New Theoretical Approaches to Strongly Correlated Systems*, NATO Science Series No. 23, edited by A. M. Tsvelik (Springer Netherlands, 2001) pp. 259–301.
[13] J. M. Tomczak, M. Casula, T. Miyake, F. Aryasetiawan, and S. Biermann, EPL **100**, 67001 (2012).
[14] R. Sakuma, P. Werner, and F. Aryasetiawan, Phys. Rev. B **88**, 235110 (2013).
[15] C. Taranto, M. Kaltak, N. Parragh, G. Sangiovanni, G. Kresse, A. Toschi, and K. Held, Phys. Rev. B **88**, 165119 (2013).
[16] J. M. Tomczak, M. Casula, T. Miyake, and S. Biermann, Phys. Rev. B **90**, 165138 (2014).
[17] P. Werner, A. Comanac, L. de Medici, M. Troyer, and A. J. Millis, Phys. Rev. Lett. **97**, 076405 (2006).
[18] K. Haule, Phys. Rev. B **75**, 155113 (2007).
[19] P. Werner and A. J. Millis, Phys. Rev. Lett. **104**, 146401 (2010).
[20] M. Casula, A. Rubtsov, and S. Biermann, Phys. Rev. B **85**, 035115 (2012).
[21] P. Sun and G. Kotliar, Phys. Rev. Lett. **92**, 196402 (2004).
[22] P. Hansmann, T. Ayral, L. Vaugier, P. Werner, and S. Biermann, Phys. Rev. Lett. **110**, 166401 (2013).
[23] A. Kutepov, S. Y. Savrasov, and G. Kotliar, Phys. Rev. B **80**, 041103 (2009).
[24] A. Stan, N. E. Dahlen, and R. v. Leeuwen, EPL **76**, 298 (2006).
[25] A. Stan, N. E. Dahlen, and R. v. Leeuwen, The Journal of Chemical Physics **130**, 114105 (2009).
[26] B. Holm and U. von Barth, Phys. Rev. B **57**, 2108 (1998).
[27] M. S. Hybertsen and S. G. Louie, Phys. Rev. B **34**, 5390 (1986).
[28] P. Rinke, A. Qteish, J. Neugebauer, C. Freysoldt, and M. Scheffler, New J. Phys. **7**, 126 (2005).
[29] M. Jain, J. Deslippe, G. Samsonidze, M. L. Cohen, J. R. Chelikowsky, and S. G. Louie, Phys. Rev. B **90**, 115148 (2014).
[30] T. Kotani, M. van Schilfgaarde, and S. V. Faleev, Phys. Rev. B **76**, 165106 (2007).
[31] S. V. Faleev, M. van Schilfgaarde, and T. Kotani, Phys. Rev. Lett. **93**, 126406 (2004).
[32] M. vanSchilfgaarde, T. Kotani, and S. Faleev, Phys. Rev. Lett. **96**, 226402 (2006).
[33] P. Koval, D. Foerster, and D. Sanchez-Portal, Phys. Rev. B **89**, 155417 (2014).
[34] J. M. Tomczak, M. van Schilfgaarde, and G. Kotliar, Phys. Rev. Lett. **109**, 237010 (2012).
[35] J. M. Tomczak, arXiv:1411.5180 [cond-mat] (2014), arXiv: 1411.5180.
[36] Z. P. Yin, K. Haule, and G. Kotliar, Nature Materials **10**, 932 (2011).
[37] K. Haule, T. Birol, and G. Kotliar, Phys. Rev. B **90**, 075136 (2014).
[38] See Supplemental Material at.
[39] A. Kutepov, K. Haule, S. Y. Savrasov, and G. Kotliar, Phys. Rev. B **85**, 155129 (2012).
[40] MQSGW is a form of quasiparticle self-consistency that replaces $\hat{\Sigma}(i\omega_n)$ with $\hat{\Sigma}(0)+i\omega_n\hat{\Sigma}'(0)$ on the Matsubara axis. It is similar to, but not identical with the form in Ref. [32] on the real frequency axis, which replaces $\langle i|\,\hat{\Sigma}(\omega)\,|j\rangle$ with $Re(\langle i|\,\hat{\Sigma}(\epsilon_i)\,|j\rangle + \langle i|\,\hat{\Sigma(\epsilon_j)}\,|j\rangle)/2$, derived from a norm minimization principle. Here ϵ_i and $|i\rangle$ are quasiparticle energy and wavefunction, respectively.
[41] H. N. Rojas, R. W. Godby, and R. J. Needs, Phys. Rev. Lett. **74**, 1827 (1995).
[42] N. Marzari, A. A. Mostofi, J. R. Yates, I. Souza, and D. Vanderbilt, Rev. Mod. Phys. **84**, 1419 (2012).
[43] F. Aryasetiawan, M. Imada, A. Georges, G. Kotliar, S. Biermann, and A. I. Lichtenstein, Phys. Rev. B **70**, 195104 (2004).
[44] D. van der Marel and G. A. Sawatzky, Phys. Rev. B **37**, 10674 (1988).
[45] A. Kutepov, K. Haule, S. Y. Savrasov, and G. Kotliar, Phys. Rev. B **82**, 045105 (2010).
[46] N. Nücker, J. Fink, B. Renker, D. Ewert, C. Politis, P. J. W. Weijs, and J. C. Fuggle, Z. Physik B - Con-

densed Matter **67**, 9 (1987).
[47] M. Jarrell and J. E. Gubernatis, Physics Reports **269**, 133 (1996).
[48] J. Ghijsen, L. H. Tjeng, H. Eskes, G. A. Sawatzky, and R. L. Johnson, Phys. Rev. B **42**, 2268 (1990).
[49] K. Haule, C.-H. Yee, and K. Kim, Phys. Rev. B **81**, 195107 (2010).
[50] F. Borsa, P. Carretta, J. H. Cho, F. C. Chou, Q. Hu, D. C. Johnston, A. Lascialfari, D. R. Torgeson, R. J. Gooding, N. M. Salem, and K. J. E. Vos, Phys. Rev. B **52**, 7334 (1995).
[51] M. Reehuis, C. Ulrich, K. Prokes, A. Gozar, G. Blumberg, S. Komiya, Y. Ando, P. Pattison, and B. Keimer, Phys. Rev. B **73**, 144513 (2006).
[52] D. Vaknin, S. K. Sinha, D. E. Moncton, D. C. Johnston, J. M. Newsam, C. R. Safinya, and H. E. King, Phys. Rev. Lett. **58**, 2802 (1987).
[53] J. M. Ginder, M. G. Roe, Y. Song, R. P. McCall, J. R. Gaines, E. Ehrenfreund, and A. J. Epstein, Phys. Rev. B **37**, 7506 (1988).
[54] S. L. Cooper, G. A. Thomas, A. J. Millis, P. E. Sulewski, J. Orenstein, D. H. Rapkine, S.-W. Cheong, and P. L. Trevor, Phys. Rev. B **42**, 10785 (1990).
[55] C. Weber, K. Haule, and G. Kotliar, Phys. Rev. B **78**, 134519 (2008).
[56] C. Weber, K. Haule, and G. Kotliar, Nat Phys **6**, 574 (2010).
[57] X. Wang, M. J. Han, L. de' Medici, H. Park, C. A. Marianetti, and A. J. Millis, Phys. Rev. B **86**, 195136 (2012).
[58] P. Werner, R. Sakuma, F. Nilsson, and F. Aryasetiawan, arXiv:1411.3952 [cond-mat] (2014), arXiv: 1411.3952.
[59] V. I. Anisimov, J. Zaanen, and O. K. Andersen, Phys. Rev. B **44**, 943 (1991).
[60] M. T. Czyzyk and G. A. Sawatzky, Phys. Rev. B **49**, 14211 (1994).